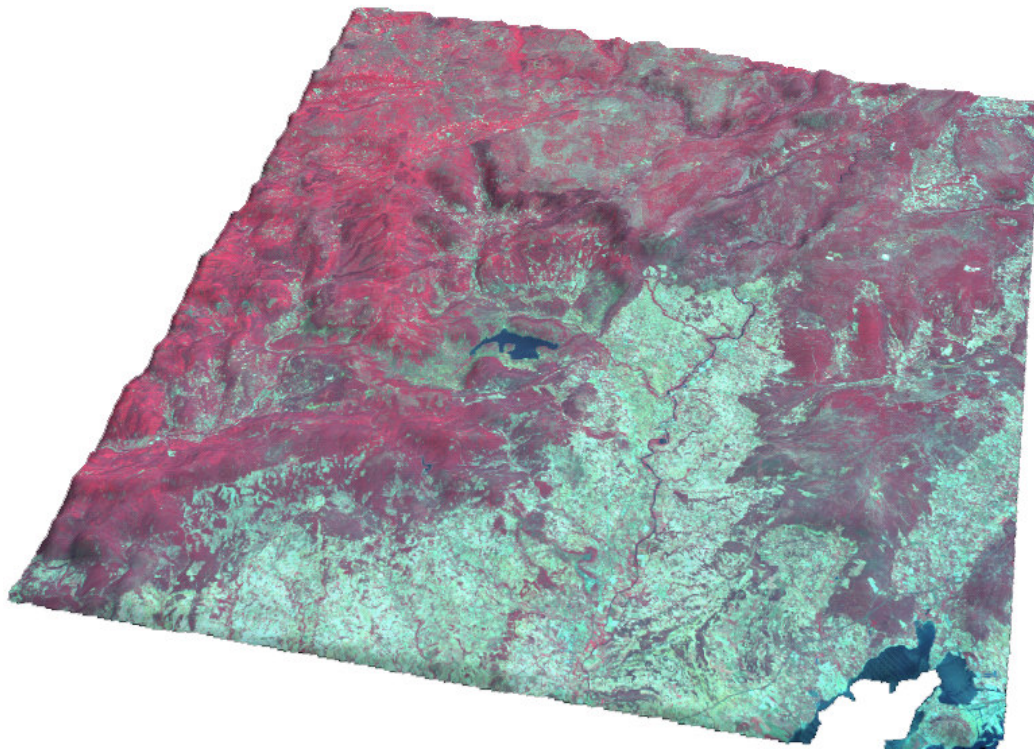
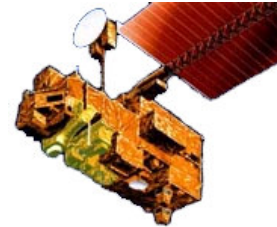


Destriping and Geometric Correction of an ASTER Level 1A Image



Rob van Ede
February 2004

Utrecht University
Faculty of GeoSciences
Department of Physical Geography
Supervisors: Prof. Dr. Steven de Jong
Drs. Raymond Sluiter



Universiteit Utrecht

Contents

	List of tables	2
	List of figures	2
1	Introduction	3
2	Introduction to thermal remote sensing	4
2.1	Blackbody radiation	4
2.2	Real-world radiation	5
3	The ASTER instrument	7
3.1	VNIR telescope	7
3.2	SWIR telescope	8
3.3	TIR telescope	8
3.4	Data Distribution: ASTER Levels	10
4	Processing of the image	11
4.1	Used ASTER image	11
4.2	Processing software	12
4.3.1	Importing image data from ASTER HDF file	12
4.3.2	Destriping	13
4.3.3	DEM generation and orthorectification	13
5	Accuracy assessment	17
5.1	Source Data: EOS/HDF file	17
5.2	Destriping	18
5.3	DEM extraction	18
5.4	Orthorectification	20
6	Usability of ASTER imagery compared to DAIS 9715 imagery for thermal mapping	21
6.1	Technical comparison ASTER versus DAIS 9615	21
6.2	Data Quality	23
6.3	Comparison of thermal products ASTER and DAIS 9615	24
7	Conclusions	28
8	References	29
	Appendix: ASTER correction HOWTO	30

List of tables:

Table 3.1:	Spectral range, resolution and bit depth (ASTER user guide)	7
Table 3.2:	Gain settings for ASTER (ASTER user guide)	9
Table 6.1:	Technical properties of ASTER and DAIS 9715 sensors	22
Table 6.2:	Summary statistics for ASTER and DAIS9715 temperature images	26

List of figures:

Figure 2.1:	Radiance of blackbody, graybody and selective radiator	5
Figure 2.2:	Location and bandwidth of ASTER bands vs Landsat 7	9
Figure 4.1:	Overall workflow for geometric and radiometric correction	11
Figure 4.2:	SWIR band 6,5,4 without and with parallax correction	14
Figure 4.3:	DEM generation from ASTER band 3N and 3B stereo pair	15
Figure 4.4:	Workflow orthorectification of VNIR and SWIR bands	16
Figure 4.5:	Workflow orthorectification TIR bands	16
Figure 5.1:	Lateral shift ASTER image	17
Figure 5.2:	Generated DEM vs IGN reference DEM and location profile	18
Figure 6.1:	Distortions resulting from non-ideal conditions in airborne remote sensing	24
Figure 6.2:	Temperature image from ASTER sensor	25
Figure 6.3:	Temperature image from DAIS sensor	25
Figure 6.4:	Differences DAIS – ASTER image	26

1 Introduction

The Advanced Spaceborne Thermal Emission and Reflection Radiometer (ASTER) is a multispectral scanner, developed by NASA, Japan's ministry of Economy, Trade and Industry (METI) and the Earth Remote Sensing Data Analysis Center (ERSDAC). The ASTER scanner features sensors for measuring reflectance and radiance in parts of the visible, shortwave infrared and thermal infrared spectrum.

Several processing steps are necessary before the data from the sensor are usable for research. What processing steps have to be performed depends on the actual usage of the data. In this paper, the radiometric and geometric correction of an ASTER Level 1A image of the Peyne catchment in Southern France will be discussed and a step by step *howto* is included in the appendix. The paper is written to answer the following question:

What corrections have to be performed on an ASTER level 1A image in order to make the image usable for further research?

In the last section, the properties of the ASTER sensor will be compared to the DAIS 9715 sensor that was used for thermal mapping of the Peyne catchment in 1998. Furthermore, a comparison of absolute temperature images on a sunny day in June from both sensors will be made.

2 Introduction to thermal remote sensing

In thermal remote sensing, radiation of objects is used to gather information on thermal properties of the objects under investigation. Thermal information of the surface provides information on moisture conditions and evapo(trans)piration. In remote sensing, the radiant temperature of an object can be measured. Radiant temperature differs from the kinetic temperature that is measured with a thermometer in direct contact with the object under investigation. The wavelengths used in thermal remote sensing are typically between 3 and 14 μm . The part between 8 and 14 μm is the most usable for thermal mapping. There are several reasons for this (Lillesand and Kiefer, 2000):

- There is an atmospheric window between 8 and 14 μm , so the atmosphere is reasonably transparent to radiation in this range.
- Peak energy emissions from objects at the earth surface occur within this range.
- The radiance in the atmospheric window from 3 to 5 μm consists of both reflected sunlight and emitted radiance from the earth surface. Both are difficult to separate.

2.1 Blackbody radiation

Every object with a surface temperature above 0 K radiates energy. This energy is radiated in a spectral distribution, typical for a material. If the object is a blackbody, the relation between the exitance peak and the surface temperature is described by *Wien's displacement law* (Lillesand and Kiefer, 2000):

$$\lambda_m = \frac{A}{T}$$

Where

λ_m = wavelength of maximum spectral radiant exitance (μm)

$A = 2898 \mu\text{m K}$

T = Temperature (K)

The *Stefan-Boltzmann law* describes the total exitance from the surface of a blackbody in all wavelengths for a given temperature. The equation is as follows (Lillesand and Kiefer, 2000):

$$M = \int_0^{\infty} M(\lambda) d\lambda = \sigma T^4$$

Where

M = total radiant exitance (W m^{-2})

$M(\lambda)$ = spectral radiant exitance ($\text{W m}^{-2} \mu\text{m}^{-1}$)

σ = Stefan-Boltzmann constant = $5.6697 \times 10^{-8} \text{ W m}^{-2} \text{ K}^{-4}$

T = temperature of blackbody (K)

As can be seen from the *Stefan-Boltzmann law*, the total radiant exitance is directly related to the temperature of the blackbody. It is therefore possible to derive the temperature from measurements on radiant exitance.

2.2 Real-world radiation

The total radiant exitance of real objects is always lower than the total radiant exitance of a blackbody, because real objects do not radiate energy in all wavelengths like a blackbody. For some objects the radiant exitance curve has the same shape as the radiant exitance curve of a blackbody, only lower. These objects radiate as a so called "graybody". Other objects have a radiant

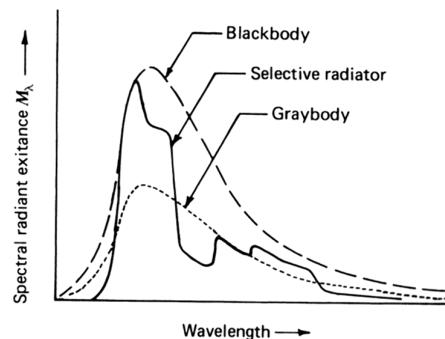


Figure 2.1: Radiance of blackbody, graybody and selective radiator (Lillesand and Kiefer, 1999)

exitance curve very different from that of a blackbody. These objects radiate as a “selective radiator”. Figure 1 shows the spectral radiance from these tree types of objects.

If we want to distillate kinetic temperatures from the measured total radiant exitance, then an extra variable has to be added to the *Stefan-Boltzmann* equation to correct for the difference in radiant exitance between a real object and a blackbody. When all objects are interpreted as a blackbody, then the measured temperatures will be lower and in some cases much lower than the kinetic temperature of those objects.

The variable that is added to the equation is the emissivity (ϵ). Emissivity describes the difference in energy radiation of an object compared to a blackbody (Lillesand and Kiefer, 2000):

$$\epsilon(\lambda) = \frac{\text{radiant exitance of an object at a given temperature}}{\text{radiant exitance of a blackbody at the same temperature}}$$

For a graybody, the emissivity is the same for all wavelengths, but always lower than 1. For a selective radiator, the emissivity changes with wavelength. When broadband sensors are used, the emissivity in the whole range of the sensor is considered constant like a graybody. For sensors equipped with multiple bands in the thermal part of the spectrum, like the ASTER for example, multiple emissivity values can be used on the different bands to improve the result. With the split-window technique for example, atmospheric effects can be derived from different emissivities in the thermal spectrum (César and Caselles, 1997). These differences in emissivity in adjacent bands are closely correlated to the water vapor content of the atmosphere and air temperature profiles. Where vegetation behaves mostly like a graybody, soils show peaks and dips throughout the spectrum (Rubio et al, 1997).

3 The ASTER instrument

The Advanced Spaceborne Thermal Emission and Reflection Radiometer is a high resolution multispectral imaging device on board of NASA's TERRA platform. TERRA was launched in December 1999 to a sun-synchronous, near polar orbit at 705 km altitude and crosses the equator at 10.30 local solar time. The orbit is the same every 16 days. Other devices on board the TERRA platform are MODIS, MISR, CERES and MOPITT.

The ASTER records data in 14 spectral bands: 3 bands in Visible Near-InfraRed (VNIR) with 15 meter spatial resolution, 6 bands in Short Wave InfraRed (SWIR) with 30 meter spatial resolution and 5 bands in Thermal InfraRed (TIR) with 90 meter spatial resolution. Detailed properties of these bands are given in table 1 and figure 2:

Subsystem	Band No.	Spectral Range (μm)	Spatial Resolution, m	Quantization Levels
VNIR	1	0.52-0.60	15	8 bits
	2	0.63-0.69		
	3N	0.78-0.86		
	3B	0.78-0.86		
SWIR	4	1.60-1.70	30	8 bits
	5	2.145-2.185		
	6	2.185-2.225		
	7	2.235-2.285		
	8	2.295-2.365		
	9	2.360-2.430		
TIR	10	8.125-8.475	90	12 bits
	11	8.475-8.825		
	12	8.925-9.275		
	13	10.25-10.95		
	14	10.95-11.65		

Table 3.1: Spectral range, resolution and bit depth (Abrams et al., 2002, <http://asterweb.jpl.nasa.gov>)

3.1 VNIR telescope

The VNIR system consists of three line arrays of 5000 CCD sensors each of which 4100 are used. Wavelength discrimination is done with a dichroic prism and interference filters. No rotating mirrors are used in the VNIR system. Each band has three gain settings for adaptation to different radiance levels without losing bit resolution (Table 2). Very different radiance levels are encountered at different location and time. In Arctic regions for example, reflection is very

high as a result of the high albedo of snow. For such a region, a low gain setting may be used to prevent the sensor from overloading. In low light conditions, a higher gain setting may be used to increase the sensitivity of the sensor and make small reflections visible. For every gain setting, there is a conversion coefficient in the telescope specific metadata to convert the digital numbers from the sensor to radiance at the sensor using the following equation (Abrams et al., 2002):

$$\text{Radiance} = (\text{DN value} - 1) * \text{conversion coefficient}$$

For DEM extraction there is another array of sensors identical to band 3, but pointed backwards. Radiometric accuracy for the VNIR system is ± 4 % or better.

3.2 SWIR telescope

The SWIR system uses a Platinum Silicide-Silicon Schottky barrier linear array of 2048 detectors for each of the six bands. For wavelength separation, optical band pass filters are used. Radiometric accuracy for the SWIR system is ± 4 % or better. Four gain settings are available (Table 2). Conversion to radiance is the same as for the VNIR bands.

3.3 TIR telescope

The TIR system uses a Newtonian catadioptric scanning system with 10 Mercury-Cadmium-Telluride detectors per band in a staggered array. Like the SWIR system, optical band pass filters are used for wavelength separation. A moving mirror is used for pointing and scanning. For calibration, there is a blackbody of which the temperature can be changed. As can be seen in Table 2, only one gain setting is available, but the TIR sensor has an increased bit depth.

Band No.	Maximum radiance ($W/(m^2 \cdot sr \cdot \mu m)$)			
	High gain	Normal Gain	Low Gain 1	Low gain 2
1	170.8	427	569	N/A
2	179.0	358	477	
3N	106.8	218	290	
3B	106.8	218	290	
4	27.5	55.0	73.3	73.3
5	8.8	17.6	23.4	103.5
6	7.9	15.8	21.0	98.7
7	7.55	15.1	20.1	83.8
8	5.27	10.55	14.06	62.0
9	4.02	8.04	10.72	67.0
10	N/A	28.17	N/A	N/A
11		27.75		
12		26.97		
13		23.30		
14		21.38		

Table 3.2: Gain settings for ASTER sensors (Abrams et al., 2002, <http://asterweb.jpl.nasa.gov>)

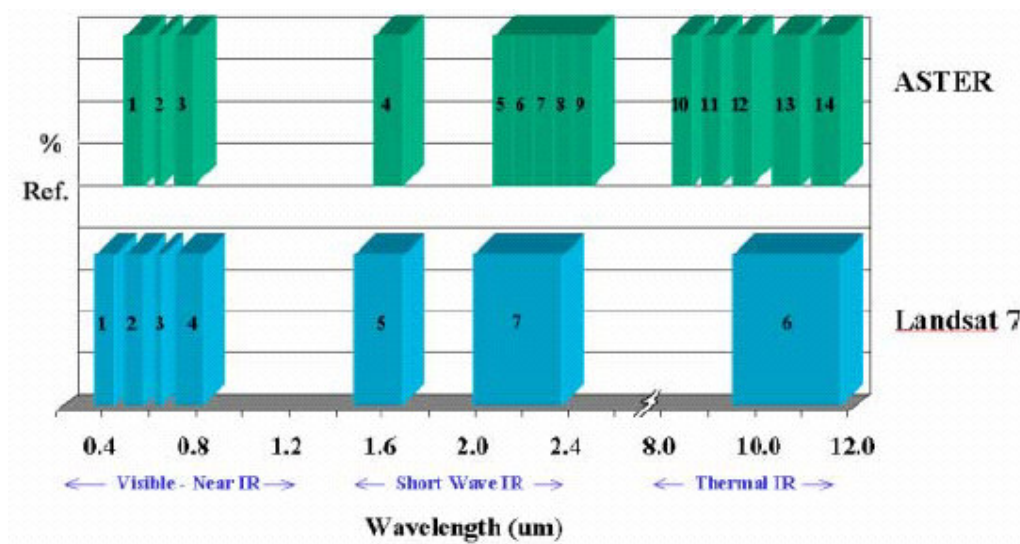


Figure 2.2: Location and bandwidth of ASTER bands compared to Landsat 7 bands (Abrams et al., 2002, <http://asterweb.jpl.nasa.gov>)

3.3 Data distribution: ASTER Levels

ASTER data are available in several processing levels. Level 1 data contain data for all bands of the ASTER instrument. Higher level data are products derived from level 1 data. There are two level one data products: Level 1A and Level 1B.

Level 1A data contain unprocessed digital counts for each band at full resolution. The coefficients for conversion to at-sensor radiance and geometric correction are supplied in the metadata, but no transformations are applied. Because no transformations have been applied, Level 1A data are a good source for DTM extraction, which will be discussed in this paper. All data collected by ASTER is processed to Level 1A data.

In Level 1B data, the raw digital counts of Level 1A data are converted to radiance values, and a transformation has been applied to register the image to a coordinate system. Because the data were resampled, level 1B data are less suitable for DTM extraction. Level 1B can however be used for spectral analysis without any preprocessing. Only cloudless scenes are processed to Level 1B.

4 Processing of the image

Before satellite imagery can be used as a data source for research of the earth surface and / or atmosphere, the raw sensor data must be processed to derive useful information from the digital numbers produced by the sensors. The most basic, but necessary processing involves geometric and radiometric correction. When these corrections are applied, the image is registered to a coordinate system, so the location of every pixel at the earth surface is known and the digital numbers are converted to radiance. This radiance values can than be converted into surface reflectance or brightness temperature.

The procedure for geometric correction and radiometric correction to at-sensor radiance is described in this paper. Correction of atmospheric effects was not performed. Because there was some striping present in some of the bands, those bands were destriped in order to remove the striping artifacts from the image data. The flowchart below (fig. 4.1) shows the overall workflow for the correction process. The different parts of this workflow will be discussed in detail in the following sections.

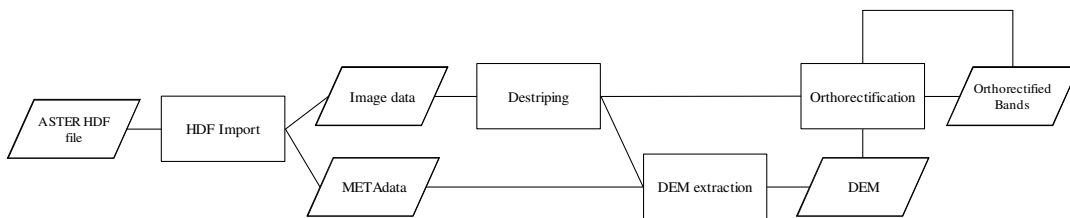


Figure 4.1: Overall workflow for geometric and radiometric correction ASTER Level 1A images

4.1 Used ASTER image

The used image is an ASTER Level 1A image of the Payne area in Southern France and was acquired on June 13th 2002. All ASTER sensors (VNIR, SWIR and TIR) were active and the image is free from clouds. Some bands suffer from striping. ASTER Level 1A image comprise a data format with no geometric and radiometric correction applied to the image. All correction coefficients are supplied in the header of the HDF file. These coefficients were extracted from the metadata and used for radiometric correction.

4.2 Processing software

All processing was carried out in two image processing programs: Erdas Imagine 8.6 (<http://www.gis.leica-geosystems.com>) and Research Systems ENVI 3.5 (<http://www.rsinc.com/envi>). Erdas Imagine has all the functionality that is needed except for rotating the image, which was done in ENVI. The destripe algorithms in both programs give different results, so for the given data, the best algorithm can be chosen.

4.3.1 Importing image data from ASTER HDF file

Erdas Imagine version 8.6 now contains an ASTER HDF importer that can do both geometric and radiometric correction of the data. Because there was some striping in the image, only the automatic radiometric correction from this import utility was used. For the automatic radiometric correction, the digital numbers are multiplied by a coefficient that depends from the gain setting of the sensor (Table 2). These coefficients are supplied in the metadata.

Striping is usually caused by some sensors that are out of alignment, defective or not calibrated correctly. This results in rows or columns in the image that deviate from neighboring rows or columns and can hamper subsequent processing. The destriping algorithms used in Imagine and ENVI were originally designed to destripe Landsat TM images that contain horizontal striping because one of Landsat's sensors was out of alignment. When the automatic geometric correction of the ASTER HDF importer is used, the image is resampled and no longer contains perfect vertical (VNIR, SWIR) or horizontal (TIR) striping (it was vertical because ASTER uses an array of sensors instead of a pointing mirror and a small number of sensors for the VNIR and SWIR bands, like Landsat). If the geometric correction of the importer is used and the image is resampled, the destriped algorithm does not work. Geometric correction thus has to be done by hand, after the striping has been removed.

4.3.2 Destriping

The destriping algorithm used in ENVI calculates the mean for each line and then normalizes the line to this mean. The periodicity of the striping is filled in as the number of sensors. For the destriping algorithm to work, the striping in the image should thus have a horizontal orientation. Because both the VNIR and SWIR sensors use an array of sensors perpendicular to the flight direction, possible striping from miscalibrated sensors will occur in a vertical orientation, and not horizontal as in Landsat images. As a result of this, the image has to be rotated prior to applying a destriping algorithm. It is best to rotate the image by 270 degrees, because the images will have the right orientation compared to each other for use in Orthobase that way. When rotated by only 90 degrees, destriping can be performed, but will not be displayed properly on Orthobase. Because the TIR sensor uses a moving mirror for scanning, the striping is already oriented horizontally and thus no rotation has to be performed.

After the rotation, actual destriping can be performed. While a different sensor is used for every column of the image (4100 sensors for VNIR, 2048 for SWIR, 700 for TIR), the number of sensors for destriping has to be set to 2. If the number of sensors is set to the actual number of sensors for each band, the output values differ considerably from the input values and data quality is compromised.

4.3.3 DEM generation and orthorectification

After the images have been destriped properly, orthorectification can be performed to georeference the images and correct for errors in image coordinates due to relief displacement, earth curvature and inter- and intra-telescope parallax errors. Especially the SWIR bands suffer from parallax errors because the sensor arrays for the different bands are not perfectly aligned. This results in bands that are shifted in space relative to each other.

In the used image, this shift was in the order of 10 pixels per band (300 meter) and thus has a very large impact on image quality if it is not corrected. When the standard geometric correction from the import-utility is used, the parallax correction is automatically applied, but then the destriping algorithms are not usable anymore (except for a Fourier Transform) as discussed in chapter 4.3.1. Figure 4.2 below shows a part of the image before correction and the edge of the image after correction so that the amount of shift needed for correction is visible.

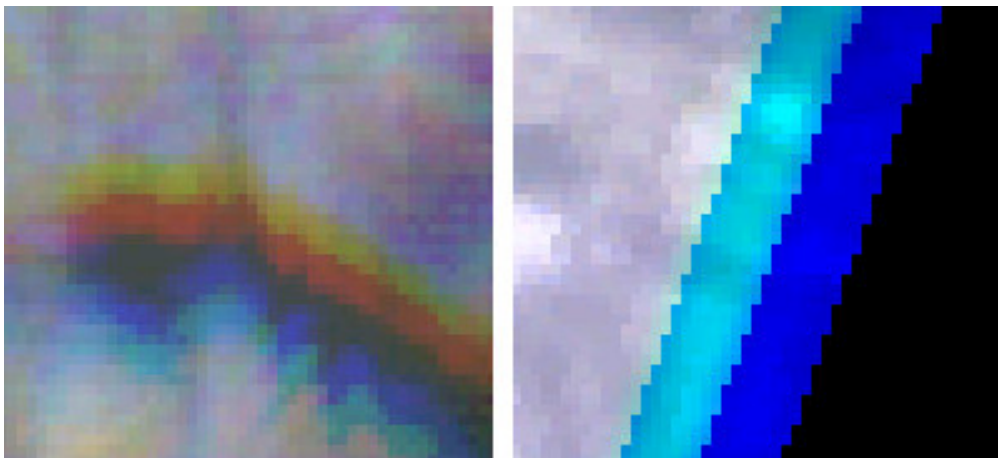


Figure 4.2: SWIR band 6,5,4 without and with parallax correction

A method for correcting for geometric errors in the image is orthorectification with a DEM (Digital Elevation Model) as input. When orthorectification is performed, all errors mentioned above are corrected in the same process. The backward looking ASTER band can be used for DEM generation, so there is no external DEM needed for the orthorectification. Erdas Orthobase pro contains all the tools for DEM extraction from stereo image sources and orthorectification. Because the DEM is needed as an input for orthorectification, the first step that has to be performed is DEM extraction. The workflow is outlined in the flowchart below (Figure 4.3):

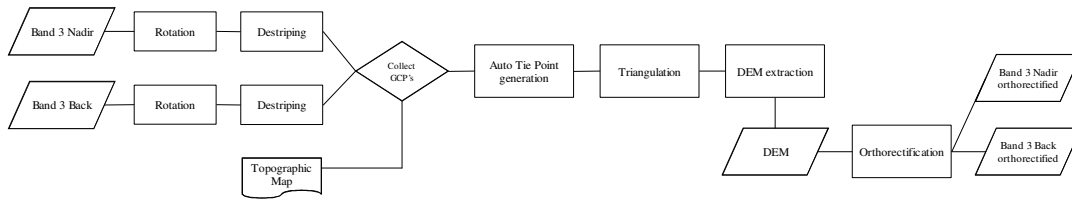


Figure 4.3: DEM generation from ASTER band 3N and 3B stereo pair

Both bands are rotated by 270 degrees so that they overlap properly.

Destriping is performed as described in paragraph 4.3.1 to remove possible striping from both images.

The value for side incidence is extracted from metadata and used for setting up Orthobase.

Ground Control Points are located from locations with known x, y and z coordinates in both images. For high quality DEM extraction from an ASTER scene, 54 to 74 GCP's are recommended (Geosystems, 2002). All GCP's were measured from topographic maps at a scale of 1:25000.

After sufficient GCP's have been located, 200 automatic tie points (Geosystems, 2002) should be generated and triangulation can be performed.

The last step is the DEM generation itself, after which the generated DEM can be used for orthorectifying the two images. The cubic convolution resampling method was used, because this method produces a sharper image than other interpolation methods. The downside of the cubic convolution method is that it applies a smoothing to the pixel values (Lillesand, Kiefer, 2000).

The orthorectified band 3N and the DEM can now be used as a source for orthorectification of the other ASTER bands. The workflow for the entire process (destriping and orthorectification) is outlined in the flowcharts below. For the thermal bands, no rotation is necessary because any striping present is already horizontal.

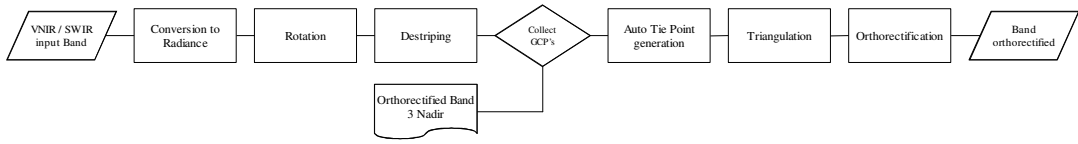


Figure 4.4: Workflow orthorectification of VNIR and SWIR bands

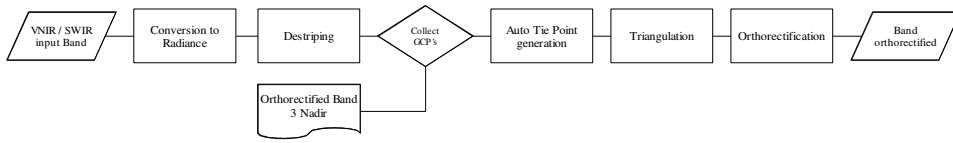


Figure 4.5: Workflow orthorectification of TIR bands

5 Accuracy assessment

The accuracy of the final product depends on the quality of the input data (rubbish in, rubbish out) and on the accuracy of all processing that is performed on the data. Therefore, every step in the workflow will be discussed in order to get some insight in the final accuracy of the end product.

5.1 Source data: HDF/EOS file:

Only images acquired by the ASTER that have low cloud coverage are normally processed to Level 1 data. Data for all bands is distributed in one HDF file and in the case of a level 1A image as discussed in this paper, the images are not georeferenced or processed to radiance. With the help of the metadata supplied in the HDF file, the image can be georeferenced and radiometric correction can be performed to get top-of-atmosphere radiance. Atmospheric conditions can have significant impact on passing radiation (absorption, scatter). This top-of-atmosphere radiance therefore can be different from the actual surface radiance and this is why it may be necessary to correct for atmospheric effects.

The coefficients for georeferencing that are supplied in the metadata have proven to be of limited use. For the global position of the image, automatic georeferencing is fine, but if the data have to be used in conjunction with other data (like in most studies), the error of several pixels is too large (figure 5.1).

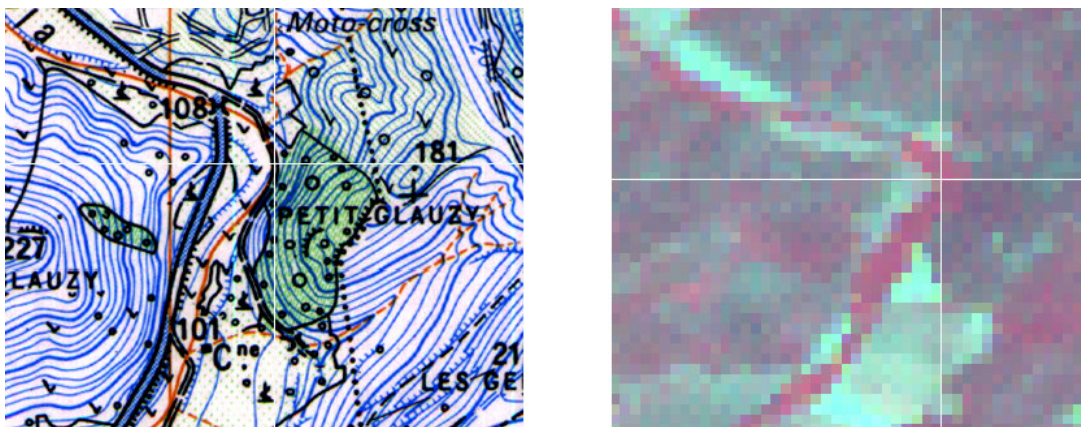


Figure 5.1: Lateral shift ASTER image (see crosshair)

Parallax errors, especially in the SWIR telescope, are another source of error that has to be corrected for (see 4.3.3), like parallax errors resulting from elevation differences.

5.2 Destriping:

Remotely sensed images often contain striping and ASTER images are no different. Especially the SWIR bands contained striping, which was reduced with a destriping algorithm from either Imagine or ENVI. The destriping algorithm in ENVI seems to work less rigorous than the algorithm in Imagine. Which algorithm should be used thus depends on the nature of the striping in the image. Only bands with heavy and uneven striping, like SWIR band 4 and the TIR bands were destriped in Imagine.

An other method for destriping, Fourier analysis, was not used because it is very labor intensive to setup and results in very long computation times.

5.3 DEM extraction:

In this paper, orthorectification on the basis of the extracted DEM was used to correct for all geometric errors. DEM extraction and orthorectification rely on the quality of the used Ground Control Points. The source for these GCPs were several 1:25.000 topographic maps. The actual quality of these maps is not known. During the measuring of GCPs, one of the used maps showed a shift of approximately 10 meters compared to the other maps and this may be one of the causes for the height exaggeration discussed below. The total RMS error for the GCPs during triangulation is 0.8664 pixels for X and 0.8391 pixels for Y. This equates to 13 meters for X and 12.6 meters for Y.

The extracted DEM has 83 meter grid cells, which is half the grid cell size that was suggested by orthobase. By using relatively large grid cells, errors from the DEM extraction are smoothed out, reducing noise. The high altitude of the spacecraft (705 km) compared to the elevation differences in the image (1 km)

makes the grid cell size of the DEM less important when it is used for orthorectification only: correction is only necessary for large terrain features that are perfectly visible in a DEM with a large grid cell size.

The extracted DEM was compared to a reference DEM with 25 meter grid cells from IGN of a part of the area. In most of the area, the generated DEM overestimates the elevation by sometimes 50 meters (figure 5.2). Close to the sea, where elevations are low, the generated DEM shows elevations below sea level where the reference DEM shows positive elevations.

From this comparison, it seems that the extracted DEM exaggerates the relief by some degree. While this may be a problem when exact heights are needed, this is much less of a problem when the DEM is used for orthorectification only, as in this paper. Overall, the extracted DEM and the reference DEM are very much alike.

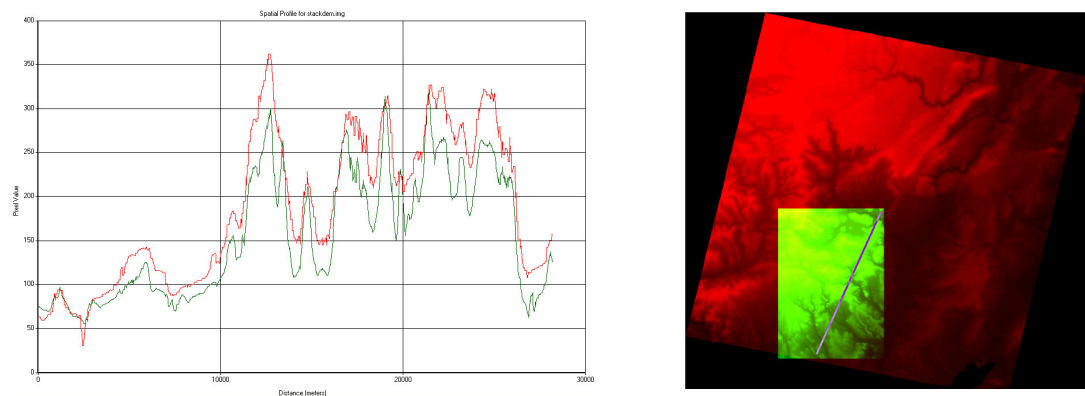


Figure 5.2: Generated DEM (red line) versus IGN reference DEM (green line) and location profile

5.4 Orthorectification:

For orthorectification, again the GCPs are important. Because some terrain features have very different reflectance / radiance properties in different bands, it is sometimes hard to identify the same feature in another band. As a result of this, the number of GCPs that can be found decreases. For orthorectification, a minimum of seven GCPs per band were used because sometimes no more reliable GCPs could be found. The coarser resolution of the SWIR and TIR bands also lowers the accuracy for the GCPs and often the middle of a pixel is used to reference a feature. In the case of features smaller

than a pixel, this feature may be positioned anywhere in that pixel and the exact location is not known. The measuring errors created by this show up during triangulation as a higher RMS error.

After orthorectification, most of the parallax errors in the SWIR bands was removed. Some very small (<1 pixel) errors remain as the result of errors from GCP measurement. This small remaining lateral shift may present a problem for spectral interpretation.

6 Usability of ASTER imagery compared to DAIS 9715 imagery for thermal mapping

From the field study carried out by Eva Koster and Arko Lucieer in 1998, extensive information is available on the thermal properties of the Payne catchment. Also, the performance of the experimental DAIS airborne scanner and the necessary processing steps for deriving the surface temperature from DAIS imagery is discussed. An ASTER image that covers the same area is now available. Having data from two scanners of the same area is an opportunity to compare the performance of both scanners. In the following sections, the comparison will be focused on the technical properties of both scanners.

6.1 Technical comparison ASTER versus DAIS 9715

While both sensors cover approximately the same wavelength range, they do so in different ways. ASTER collects data in three atmospheric windows: VNIR, SWIR and TIR. DAIS collects data in four atmospheric windows: VNIR, SWIR, MIR and TIR. ASTER uses only 14 relatively wideband sensors, while DAIS uses 79 sensors. Some of the DAIS bands are very narrow, while others cover a larger bandwidth.

The spatial resolution is the same for all bands of the DAIS sensor, which means that data for every covered wavelength are available at the same pixel size. In this way, it is relatively easy to link for example optical to thermal data. ASTER uses a different spatial resolution for the different wavelength ranges. This means that data are collected at different resolutions and some additional processing is required to link these data.

For the VNIR and SWIR bands, ASTER utilizes no rotating mirrors, but a separate sensor for each pixel. This absence of rotating parts guarantees a consistent quality throughout sensor life, not compromised by mechanical wear or vibrations. The use of many sensors requires all sensors to be calibrated very accurately, or striping will occur in the way described above. The moving mirrors used in the DAIS sensor are susceptible to vibration, for

example from the engine of the airplane in which it is installed (Strobl, 1996). This also results in striping.

In table 6.1, the technical properties of both sensors are listed:

	ASTER	DAIS 9715
Number of bands	VNIR: 3 + back looking SWIR: 6 TIR: 5	VNIR: 32 SWIR1: 8 SWIR2: 32 MIR: 1 TIR: 6
Spatial resolution	VNIR: 15 m SWIR: 30 m TIR: 90 m	depends on altitude, identical for all channels typically 7 m (at 3000 m altitude)
Wavelength range	VNIR: 0.52 – 0.86 μm SWIR: 1.60 – 2.43 μm TIR: 8.125 – 11.65 μm	VNIR: 0.4 – 1.0 μm SWIR1: 1.5 – 1.8 μm SWIR2: 2.0 – 2.5 μm MIR: 3.0 – 5.0 μm TIR: 8.7 – 12.3 μm
Bandwidth	VNIR: 0.60 – 0.80 μm SWIR: 40 – 70 nm TIR: 0.35 – 0.70 μm	VNIR: 12 – 35 nm SWIR1: 36 – 56 nm SWIR2: 20 – 40 nm MIR: 2.0 μm TIR: 0.6 – 1.0 μm

Table 6.1: Technical properties of ASTER and DAIS 9715 sensors (collected from Abrams et al., 2002 and Strobl, 1996)

6.2 Data quality

The data acquired by both sensors do not only differ in quantity, but also in quality. In remotely sensed images, distortion may be of geometric or radiometric nature. Radiometric distortion can be caused by instrument miscalibration or atmospheric effects (Lillesand and Kiefer, 2000). When an instrument uses sensors that work reliably and as specified, lookup tables can be used to retrieve data with good radiometric quality.

The radiance measured by the sensor is called the at-sensor radiance. The atmosphere between the sensor and the earth surface has influence on passing radiation, and thus on the final measurement. As the DAIS sensor was operated from an airplane at an altitude of 3000 meter and ASTER is onboard the TERRA platform at an altitude of 705.000 meter, there is much more atmosphere between ASTER and the earth surface than there is between DAIS and the earth surface. A longer path through the atmosphere means more potential influence of the atmosphere on the radiation that has to be corrected for. There are different methods for atmospheric correction. One simple method is the darkest pixel method, in which the value of a pixel that is assumed to be black (like deep, clear water) is subtracted from all pixels in that band. Another method, that requires field measurements, is the empirical line method. In the empirical line method, field measured reflectance / exitance values are used to remove atmospheric influence in the image using linear regression. A third method for atmospheric correction is a computer based model such as MODTRAN or ACORN. These models require additional information on atmospheric conditions when the image was acquired and thus, more uncertainties are introduced. The required additional data for ACORN are atmospheric visibility and fixed water vapor (ImSpec, 2002).

Because DAIS is an airborne scanner and ASTER is onboard a spacecraft, ASTER moves in a more steady and predictable way than DAIS, which is much more prone to variations in the flight path. Figure 6.1 shows these variations, along with the resulting geometric errors in the recorded image. In spaceborne remote sensing, these problems do not exist.

Vibrations from the airplane may have influence on data quality. Severe striping in some of the SWIR bands in the DAIS image was caused by vibrations of the engines (Strobl, 1996).

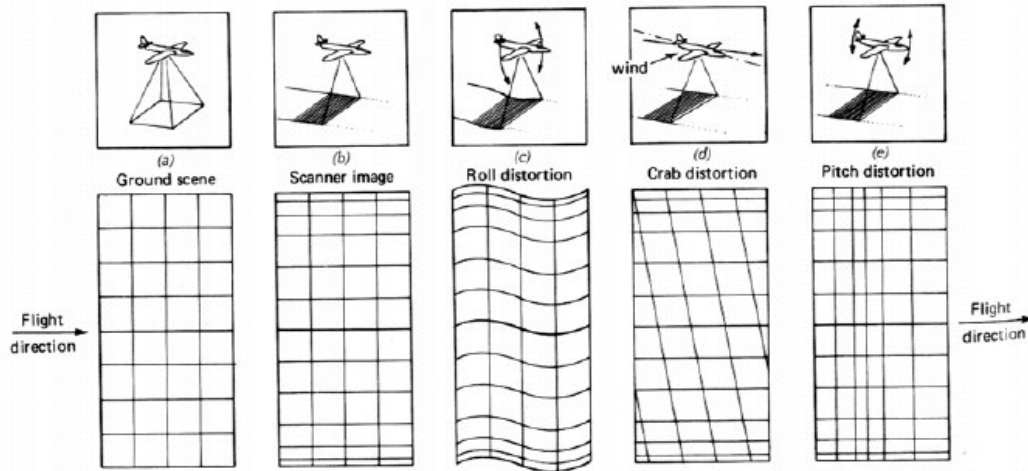


Figure 6.1: Distortions resulting from non-ideal conditions in airborne remote sensing (Lillesand and Kiefer, 2000)

6.3 Comparison of thermal products ASTER and DAIS

To gain insight in differences in usability of thermal data from the ASTER or DAIS sensor, two extracted absolute temperature images will be discussed below, as well as possible methods for extraction of these images.

Both ASTER and DAIS sensors record thermal data in several bands. Methods that may be used for extraction of surface temperature therefore are the same. Methods for temperature extraction that use data in all thermal bands are: Emissivity Normalization and Temperature Emissivity Separation, which is used to convert radiance data to the ASTER Level 2 Surface Kinetic Temperature data product.

Although the ASTER image was taken one year after the DAIS image, both were taken on a sunny day and observed temperatures are comparable. Because the conditions on both days were not exactly the same and atmospheric properties such as visibility and atmospheric water vapor are not known, no atmospheric correction was performed on radiance values from the ASTER sensor. Actual temperatures therefore will be higher than the

calculated temperatures. This is acceptable because extracted temperatures are only used for assessment of relative differences.

For the ASTER sensor, temperatures were calculated using the Emissivity Normalization method: a fixed emissivity is chosen that is used to calculate temperatures from each band. The band resulting in the highest temperature is used. This process is repeated for all pixels. When the temperature is known, emissivity can be calculated for each band and every pixel as well.

Temperatures from the DAIS sensor were calculated by Lucieer and Koster using the empirical line method, as discussed above.

In figures 6.2 and 6.3, the ASTER and DIAS temperature images are shown. On a large scale, both images show the same information: Large terrain features with differing temperature can be distinguished without difficulties. The larger pixel size of the ASTER sensor however, results in loss of detail. In theory, objects of comparable size as the pixels should be detectable. Because terrain features only rarely fit exactly within one pixel, parts of these features are registered in one pixel and other parts in other pixels. Registered exitance of several objects within one pixel is averaged over the entire surface of this pixel. The result of these “mixed pixels” is that detection of objects even larger than the pixel size is problematic. In figure 6.2 and 6.3, this effect is best visible in the bottom part, where fields clearly larger than several pixels in

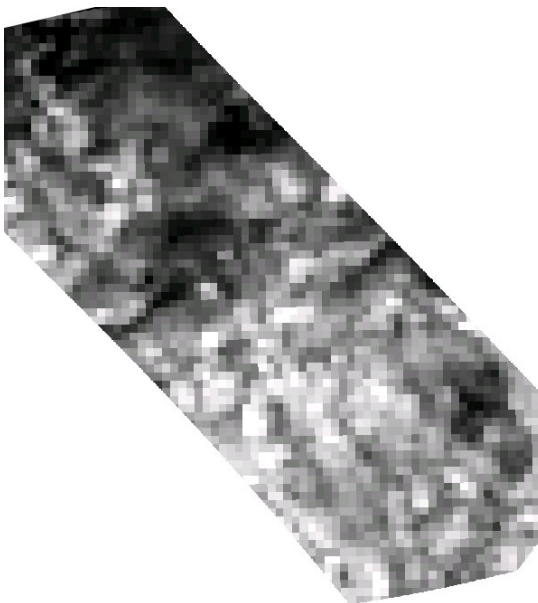


Figure 6.2: Temperature image from ASTER sensor



Figure 6.3: Temperature image from DAIS sensor

the ASTER image are not distinguishable from the surrounding fields. When both images are subtracted, the amount of detail that is lost remains. Figure 6.4 shows this loss of detail.



Figure 6.4: Difference DAIS – ASTER image

In table 6.2, below, summary statistics for both images are shown. The higher spatial resolution of the DAIS sensor is reflected in the larger standard deviation and the more extreme high and low values that are recorded. In the ASTER image, extreme temperatures from small objects are averaged within the pixels, resulting in filtered-out extremes and thus a lower standard deviation.

	ASTER	DAIS9715
Min	30.7	22.2
Max	39.5	62.1
Mean	35.7	34.8
Median	35.7	35.2
Standard deviation	1.2	5.7

Table 6.2: Summary statistics for ASTER and DAIS9715 temperature images

Which sensor is most usable depends on the intended usage of the data. When detailed information on smaller objects is needed, the DAIS sensor is the sensor of choice. Being an airborne sensor, considerable work has to be done on geometric correction of the image data. Because the limited field of view, several images must be stitched when a larger coverage is needed. When research is performed on larger scale features, such as soil moisture or large scale temperature measurements, an ASTER image may be all that is needed, with the added benefit of larger data granules and greater geometric integrity.

7 Conclusions

- Removal of striping from ASTER bands can be done effectively with both Erdas Imagine and ENVI.
- Geometric correction coefficients supplied in the metadata are not reliable enough for precision mapping. Ground Control Points are needed for accurate georeferencing of the images. The number and quality of the available Ground Control Points is also the greatest point of uncertainty in the here presented process of rectifying an ASTER image.
- SWIR bands suffer from major parallax errors that result in a lateral shift up to 300 meters that must be corrected for. After correction, a small lateral error remains that may be a problem for spectral interpretation upon use of the image.
When level 1B data are used, correction for these errors has already been carried out.
- The generated DEM shows relief exaggeration and should therefore not be used as an absolute DEM.
- Space borne sensors are less susceptible to gross geometric errors from variations in the flight path than airborne sensors like DAIS. Atmospheric influence however, is larger for spaceborne sensors.
- The higher spatial resolution of the DAIS sensor compared to the ASTER sensor is not only reflected in higher image detail, but also in greater differences between highest and lowest measured temperatures.

References

Abrams, M., Hook, S., Ramachandran, B., 2002. ASTER User Handbook, ver. 2. Jet Propulsion Laboratory, EROS Data Center

Coll, C., Caselles, V., 1997. A split-window algorithm for land surface temperature from advanced very high resolution radiometer data: Validation and algorithm comparison. *Journal of Geophysical Research* 102:16,697-16,713

ERDAS Field Guide, 1999. ERDAS Inc., Atlanta, U.S.A.

ERSDAC, 1996. Algorithm Theoretical Basis Document for ASTER Level-1 Data Processing, ver. 3.0. Earth Remote Sensing Data Analysis Center, USA

Geosystems, 2002. DEM and Orthoimage from ASTER. Germering, Germany

ImSpec LLC, 2002. ACORN 4.0 Tutorial. Boulder, USA

Lillesand, T.M. & Kiefer, R.W., 2000. *Remote Sensing and Image Interpretation*, John Wiley & Sons, New York, 750 pp.

Koster, E., Lucieer, A., 2000. The DAIS La Payne Experiment: Using the Optical and Thermal DAIS Bands to Survey and Model the Surface Temperature. Utrecht University, The Netherlands

Rubio, E., Caselles, V., Badenas, C., 1997. Emissivity Measurements of Several Soils and Vegetation Types in the 8-14 μm Wave Band: Analysis of Two Field Methods. *Remote Sensing of Environment* 59:490-521.

Strobl, P., Richter, R., Lehmann, F., Mueller, A., Zhukov, B., Oertel, D., 1996. Preprocessing for the Digital Airborne Imaging Spectrometer DAIS7915. *SPIE Proceedings* 2758:109-117 (in Koster & Lucieer)

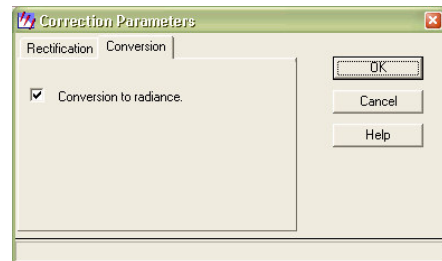
Appendix: ASTER correction HOWTO

Below, the procedure for geometric and radiometric correction for the ASTER image discussed in this paper is described step by step. Some parts of the processing will be performed in *ERDAS Imagine*, other parts in *Research Systems ENVI*.

EOS/HDF import (Imagine):

The following steps should be repeated for every band that is to be imported.

- Select **Import** from the Imagine toolbar.
- As *file type*, select **ASTER EOS HDF Format**.
- Select **file** in the *media* dropdown list.
- Browse to the HDF file to be imported and provide the location and file name for the output image, click **OK**. The output file will have the “*img*” extension.
- Select the band of to be imported using **Previous** and **Next Image** buttons.
- Use the **Correction** button and select **Convert to Radiance** on the *Conversion* tab to automatically convert the digital numbers in the image to radiance at-sensor using the ASTER gain settings from the metadata. A GCP file can be produced by selecting **Write GCP file** on the *Rectification* tab, but this is not necessary for further processing. The **Write Transform to Image** option should not be used because destriping of the image as described in this document will be impossible then.
- Click **OK** and the selected band will be imported.

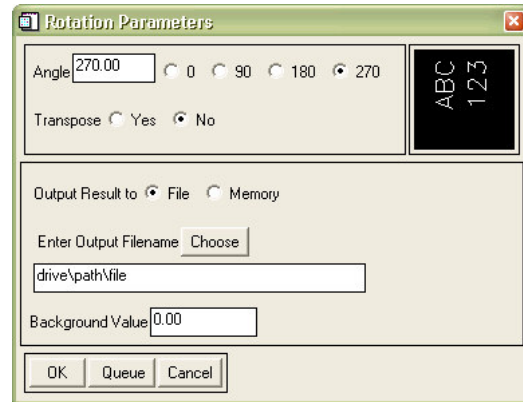


After the images are imported, make a note of the sensor’s side incidence that will be needed in Orthobase later. This value can be found in the *HDFGlobalAttributes* tab in the *Layer Info* dialog (*Viewer – Utility – Layer Info...*). The sign of this value should be changed (must be positive).

Rotating the images (ENVI):

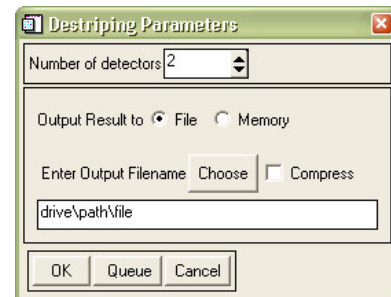
To prepare the images for destripping and for proper display in *Orthobase* later, all of the images from the VNIR and SWIR telescopes (bands 1 - 9) should be rotated 90 degrees counter clockwise (=270 degrees clockwise). The TIR bands should not be rotated prior to destripping.

- Select *Basic Tools* – **Rotate / Flip Data** from the ENVI menu bar.
- Select the file to be rotated from the list, or use the **Open File....** button to browse to the desired file, click **OK**.
- Fill in 270 degrees in the *Angle* box.
- Choose the output location and file name in the *Enter Output Filename* box, click **OK** to perform the rotation.



Destripping the images (ENVI):

- Select *Basic Tools* – *General Purpose Utilities* – **Destripe** from the ENVI menu bar.
- Select the desired input file from the list and click **OK**.
- Set the *Number of detectors* to 2.
- Choose the output location and file name in the *Enter Output Filename* box, click **OK** to destriped the image.



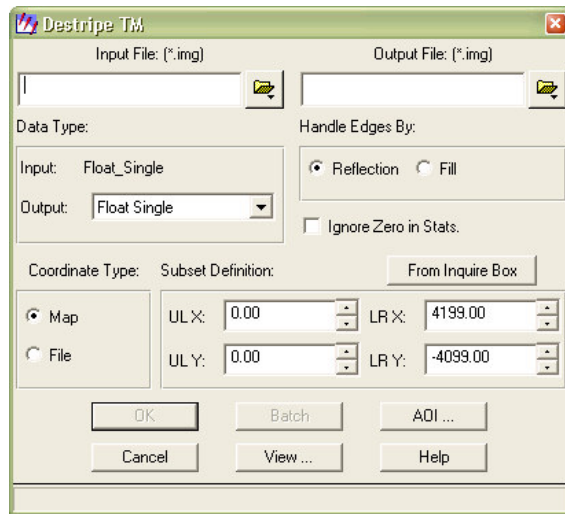
Importing the ENVI images in Imagine (Imagine):

Because the ENVI file format cannot be read by Imagine, the images should first be imported again.

- Select **Import** from the Imagine toolbar.
- As *file type*, select **ENVI (Direct Read)**.
- Select **file** in the *media* dropdown list.
- Fill in the input and output fields and click **OK** to import the images.

Carefully examine all images for any striping that might still be present. If there is still striping in an image, this can be removed with the destripe utility of Imagine:

- Select **Import** from the Imagine toolbar.
- Select **Radiometric Enhancement**
- Select **Destripe TM Data**
- Fill in the input and output fields and click **OK** to destripe the image.



Orthorectification of the images (Imagine - OrthoBASE):

- Select **OrthoBASE** from the Imagine toolbar.
- Create a new OrthoBASE project.
- Select the location and name of the to be created *block file*.
- Select **Generic Pushbroom** from the Model Setup Dialog.
- Click the **Set Projection** button and select the desired projection for the orthorectified images.
- Click **Next** and select the desired horizontal and vertical units, click **OK**.

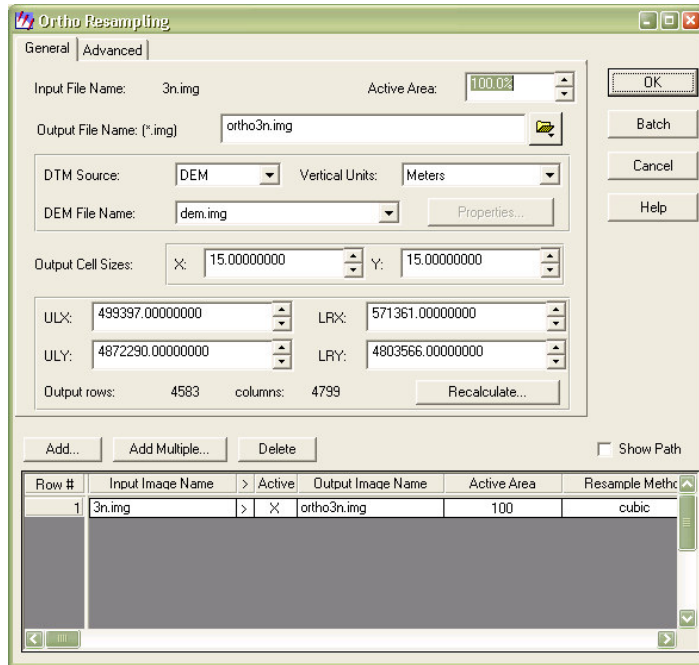
- Load band 3nadir and band 3backward by clicking *Edit – Add Frame...* and browsing to the rotated and destriped images for band 3.
- Click *Edit – Frame Editor...* to open the Frame Editor dialog.
- Click the **New** button and fill in the parameters in the *General* and *Model Parameters* tab (GeoSystems, 2002), click **OK** when done:

GENERAL		
Sensor Name	ASTER VNIR nadir	ASTER VNIR backward
Focal Length (mm)	329.0	329.0
Principal Point x0 (mm)	0.0	0.0
Principal Point y0 (mm)	0.0	0.0
Pixel Size (mm)	0.007	0.007
Sensor Columns	4100	5000

MODEL PARAMETERS		
Polynomial Orders of Sensor Model		
X	2	2
Y	2	2
Z	2	2
Omega	1	1
Phi	1	1
Kappa	2	2

- In the *Frame Attributes* tab, fill in the value for *Side Incidence* that was found in the metadata before. Leave the *Track Incidence* 0 (for the backward image –30.96), set the *Ground Resolution* to 15 meters and *Sensor Line Along Axis* to y (GeoSystems, 2002).
- Click *Edit – Compute Pyramid Layers* to create pyramid layers for all images without them.
- Use the *Point Measurement Tool* (*Edit – Point Measurement*) to measure as much *Ground Control Points* as possible: >54 (GeoSystems, 2002).
- Click *Edit – Auto. Tie Point Generation Properties...* , set the *Initial Type* to “Tie Point” and the *Intended Number of Points per Image* to 200, click **Run** and **OK** to generate the Tie Points.
- In the *Advanced Options* tab of the *Triangulation* Dialog (*Edit – Triangulation Properties*), disable the **Simple Gross Error Check** option after all GCPs have been checked visually, and enable the **Consider Earth Curvature in Calculation** option. Click **Run** to perform the Triangulation and then **OK**.

- For DTM extraction, click *Process – DTM Extraction*, and choose the desired filename and cell size for the extracted DTM.
- Click *Process – Orthorectification – Resampling* to bring up the orthorectification box.
- Fill in the filename for the orthorectified image in the *Output File Name* box.
- Choose **DEM** from the *DTM Source* dropdown list and fill in the location and file name of the DTM that was created before in the *DEM File Name* box.
- Fill in the desired cell size for the orthorectified image. For the VNIR bands, this is 15 meters.
- The *Resampling Method* can be changed in the *Advanced* tab.
- Click **OK** to start the orthorectification process.



The orthorectified image that is created for the nadir-looking band 3 can now be used as a reference for orthorectification of the other bands. Because the VNIR, SWIR and TIR bands of ASTER use different cell sizes, three *Orthobase block-files* should be created. The procedure is the same as described above, except for some band-dependent settings. These differences will be pointed out below:

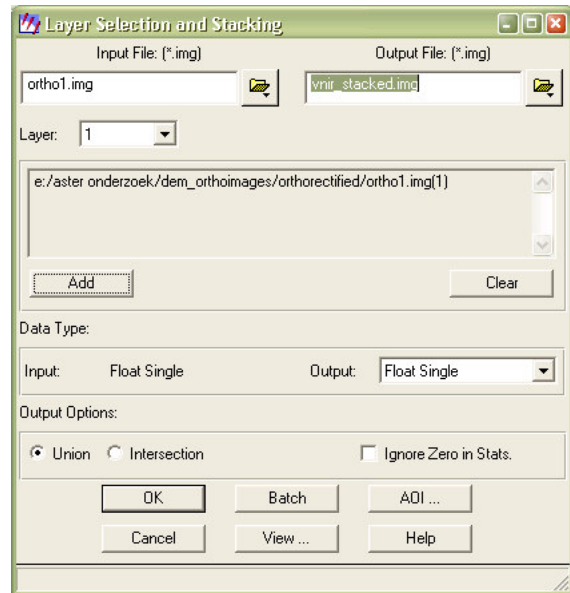
- In the *Sensor Parameters* dialog (*Edit – Frame Editor - NEW*), the value *Sensor Columns* should be set to 4100 for the VNIR bands, 2048 for the SWIR bands and 700 for the TIR bands. In the *Frame Attributes* tab, the *Ground Resolution* should be set to 15 m for the VNIR bands, 30 m for the SWIR bands and 90 m for the TIR bands. The *Sensor Line*

Along Axis should be set to “y” for both the VNIR and SWIR bands and set to “x” for the TIR bands.

- During the measurement of GCPs, the already orthorectified band 3n image may be used as reference.
- No DTM can be generated, but the DTM file that was created earlier can be used for orthorectification of all images.

When the images of all bands have been orthorectified, the separate files can be combined to form a single, multi-layer file per telescope. Because of the different cell sizes for the different telescopes, it is not advisable to stack all 14 bands in one file. For stacking the images for the VNIR, SWIR and TIR telescopes, the *Layer Stack* utility can be used:

- Select *Interpreter – Utilities – Layer Stack...* from the Imagine toolbar.
- Select the first orthorectified image to be stacked in the *Input File* box and click the **Add** button. Repeat this for the other files to be added to the stack (1 – 3 for the VNIR telescope).
- Fill in the location and filename for the to be created stacked file.
- Click **OK** to start the process.
- Repeat this process for the SWIR and TIR bands.



When all steps mentioned above have been followed, you now have three destriped , orthorectified multi-layer image files with at-sensor radiance values and a DTM.